Modelling and experimental characterisation of a compressional adaptive magnetorheological elastomer isolator

Journal Title
XX(X):1–15

DOI: 10.1177/ToBeAssigned
www.sagepub.com/
SAGE

Emiliano Rustighi[1,3], Diego Francisco Ledezma-Ramirez[2], Pablo Ernesto Tapia-Gonzalez[2], Neil Ferguson[3] and Azrul Zakaria[3]

Abstract

This paper proposes a simple physical-based model to describe and predict the performance of axially compressed magnetorheological elastomeric (MRE) cylinders employed as vibration and shock absorbers. The model describes the MRE macroscopic stiffness changes due to an externally applied magnetic field from a microscopic composite cell of silicone rubber and carbonyl iron particle. Despite neglecting the material hyperelasticity, anisotropy and adjacent magnetic interaction, the model describes effectively the effect of the magnetic field on the macroscopic modulus of elasticity. The changes in the mechanical properties with the induced magnetic field are measured on samples of different particle concentration based on volume percentage, i.e. ten and thirty percent concentration of iron particles in a silicone rubber matrix. The manufacturing process of the samples is detailed, as well as the experimental validation of the effective stiffness change under a magnetic field in terms of transmissibility and mobility testing. However, the prediction seems to be limited by the linear elastic material model. Predictions and measurements are compared, showing that the model is capable of predicting the tunability of the dynamic/shock absorber and that the proposed devices have a possible application in the reduction of mechanical vibrations.

Keywords

magnetorheological, elastomer, vibration isolation, smart materials

Introduction

Magnetorheological elastomer (MRE) is a class of material that consists of a polymeric matrix with embedded ferromagnetic particles such as carbonyl iron particles (CIPs). Since its mechanical properties change very rapidly by the application of a magnetic field, the magnetorheological elastomer became a widely used material when it comes to controllable features applied to active and semiactive vibration control and suppression. A comprehensive review of MRE has been presented by Li et al. (2014) discussing the fundamental theory of these materials, manufacturing methods, configurations and applications. Some of the most relevant works are briefly explained here.

Modelling of MREs has focused on predicting how the MRE elastic properties change with the induced magnetic field. Dipole-dipole magnetic particle interaction model was used firstly by Jolly et al. (1996) to describe the increase in shear modulus in a suspension of ferromagnetic particles in a non-magnetic matrix as a magnetic field is applied perpendicular to the strain direction. Overall, under small strain condition, the dipole-dipole magnetic particle interaction model is efficient and mathematically concise. The same model has been utilised over the years by Davis (1999), Shen et al. (2004), Chen and Jerrams (2011) and Li and Sun (2014) to describe the magnetic field dependency of MRE shear modulus. These papers only differ on the approaches for computing the zero-field shear stiffness; namely finite element model, hyper elastic rubber model,

[1]University of Trento, Department of Industrial Engineering, Italy
[2]Universidad Autónoma de Nuevo León, Facultad de Ingeniería Mecánica y Eléctrica, Mexico
[3]University of Southampton, Institute of Sound and Vibration Research, UK

Corresponding author:
Emiliano Rustighi, University of Trento, Dipartment of Industrial Engineering, via Sommarive 9, 38123 Trento, Italy
Email: emiliano.rustighi@unitn.it

standard linear solid and viscoelastic interfaces respectively. Subsequently more complicated models, which are based on magnetic-mechanical microstructure, have been developed (Borcea and Bruno 2001; Yin et al. 2002; Wang et al. 2003; Dorfmann and Ogden 2004; Yin and Sun 2005; Yin et al. 2006; Bustamante 2010; Castañeda and Galipeau 2011; Danas et al. 2012; Han et al. 2013) to consider both zero-field and magnetic-field dependency on the shear modulus of the MRE composites. These models provide the shear and Young's modulus of MRE as a magnetic field is applied perpendicular to the load surfaces.

Experimental work has been carried out concurrently by separate research groups. Brigadnov and Dorfmann (2003) showed that the effect of the magnetic field is to stiffen the shear response of the material. They conducted mathematical modelling of MRE by using the concept of the strain-energy functions. The derivation of the equations were based on a model of MRE confined by parallel top and bottom plates, which is subjected to shear deformation under the influence of a magnetic field normal to the plates. An acceptable agreement was achieved between the numerical simulation and experimental results. Blom and Kari (2005) indicated that the magneto-sensitive effect of MR rubber is also dependent on its amplitude and frequency. From experimental results, rubber samples in the audible frequency range showed that both the magnitude and loss factor of the shear modulus are strongly amplitude dependent. These results also concluded that introducing iron particles into the rubber increase its amplitude dependence over the entire frequency range. Wang et al. (2006) investigated the effects of interactions between CIPs and a silicone rubber matrix, on the performance of MRE related to MR effect and mechanical properties. By utilising silane coupling agents during the mixing process, it was seen that improvement in dispersion of the iron particles and the interaction between iron particles and the matrix is possible, thus increasing the tensile strength of the MRE. Stepanov et al. (2007) conducted elongation, static and dynamic shear experiments to study MRE behaviour in the presence of a homogeneous magnetic field. It was found that the elastic modulus increased as an external homogeneous magnetic field increases up to 0.3 T (Tesla).

Other researchers mainly focused on the design of MRE smart devices. Deng and Gong (2008) developed an adaptive tuned vibration absorber (ATVA) by utilising MRE as its smart spring elements. From the theoretical and experimental results, the developed ATVA performed a frequency shift from 27.5 Hz to 40 Hz and it showed vibration absorption capability up to 25 dB. Blom and Kari (2012) utilised MR material in the form of rubber bushing and investigated its property with the influence of frequency, amplitude and magnetic field. The frequency and amplitude dependent stiffness of the bushing were modelled based on geometric dimensions and shear modulus. From the results presented, it can be seen that the the stiffness of the bushing can be controlled over a large range of the applied magnetic field strength.

An interesting application of MRE is the control and suppression of vibrations using switchable stiffness due to their characteristics of being able to rapidly change between low and high stiffness states. This can be particularly suitable for on off switching stiffness strategies for shock and vibration isolation and suppression (Ledezma-Ramirez et al. 2012, 2011). More recently, MRE have been applied in sandwich beams using rectangular control functions leading to faster dissipation of transient vibrations (Eshaghi et al. 2016; Dyniewicz et al. 2015; Landi et al. 2019).

Based on the previous literature overview, the main contribution of the paper is to to provide a simple physical-based model to predict the compressional stiffness changes due to a magnetic field aligned with the MRE element, following the model proposed by Jolly et al. (1996). First, the material samples and their manufacturing process is presented since this will be used to present analytical and numerical results. Then the stiffness of the composite in the absence of a magnetic field is predicted from the properties of the matrix and of the particles, which in this particular application are silicone rubber and carbonyl iron particles (CIPs) respectively. The effect of the magnetic field is quantified and a nonlinear constitutive equation for the magnetic field given. In order to calculate the latter, the magnetic induction in the MRE element is computed. Eventually, a relationship for the linearised stiffness around the equilibrium position given as a function of the magnetic field, and the vibration isolation and absorption properties are obtained from the transmissibility and impedance functions. The second part of the paper presents the experimental characterisation of the MRE samples in order to show the usefulness of the model by assessing the stiffness change under the influence of a magnetic field and the applicability of the material into vibration control devices. The natural frequency and damping are obtained by shaker excitation for different configurations, and transmissibility and impedance functions are presented. The shock isolation properties are also briefly considered. The paper finishes with a general discussion of the theoretical and experimental findings, highlighting the

possibilities for further developments of semiactive stiffness control strategies for vibration and shock control.

Material samples manufacturing

The MRE samples manufactured and tested in this paper have been made using silicone rubber (MM288 by ACC Silicones Ltd) as matrix and carbonyl iron powder (CIP Type SQ by BASF SE) as ferromagnetic particles. Type SQ CIP consists of a fine, grey soft iron powder particles which are spherical in shape with an average diameter of 5 μm and with a 99.5% iron content purity. Density of the carbonyl iron particle, ρ_{CIP}, and the silicone rubbber, ρ_{SR}, are 7.874 g/cm^3 and 1.12 g/cm^3 respectively. Silicone rubber was chosen since it is easy to use and possesses good properties such as very good chemical and UV resistance in a wide temperature range (Schubert 2014). Iron particles were chosen because of their low remnant magnetisation, high permeability and high saturation magnetisation (Lokander and Stenberg 2003). Due to these properties, high magnetorheological effects can be obtained as a result from better inter-particle interaction (Carlson and Jolly 2000).

The MM288 silicone rubber kit comprises two components, namely the rubber and the hardener which have been mixed together with a 10:1 ratio. The desired percentage of CIP was added first to the silicone rubber, then the hardener was added as the last component. As recommended by the supplier, no additive was required for the MM228 kit since the viscosity of the silicone rubber is relatively low in comparison to the one of other materials used in MRE (Schubert 2014). The mixture was placed into a vacuum chamber for 10 minutes to remove any trapped air inside the mixture. After this degassing process, the MRE mixture was poured into an aluminium mould. All surfaces of the mould in contact with the mixture were sprayed with silicone release agent for ease of removing the MRE from the mould. The rubber was cured at room temperatures for 24 hours although the curing process can be accelerated by heating (curing at 100°C takes only 30 minutes).

Each sample is in the form of a cylinder with a 30 mm diameter and a 12 mm height. Samples with a CIP volume percentage of 0, 10 and 30% have been manufactured and tested. Table 1 shows the material properties of the silicone rubber and of the CIP.

Table 1. Material parameters.

	Description	Value
E_{SR}	Young's modulus silicone rubber	1.013 MPa
ν_{SR}	Poisson ratio silicone rubber	0.45
E_{CIP}	Young's modulus Carbon Iron Powder	211 GPa
ν_{CIP}	Poisson ratio Carbon Iron Powder	0.33

Modelling

In this section a constitutive model of the MRE, able to predict the change in the effective compressional modulus of elasticity due to exposure to an aligned external magnetic field, is proposed. First, the effective modulus of elasticity for the composite MRE, assumed to be an homogeneous and isotropic suspension of metal spherical particles into the elastomeric matrix is considered. Next, following the approach proposed by Jolly et al. (1996) for magnetorheological fluids, the magnetic induction in the metal spherical particles and in the elastomeric matrix is calculated taking into consideration an elemental cell of the MRE. Consequently, the magnetic constitutive response of the MRE is obtained. Finally, since the obtained stress-strain curves are highly nonlinear, the linearised effective elastic modulus around an equilibrium position is calculated for the subsequent linear vibration response predictions.

Elasticity of the MRE composite

In order to calculate the MRE composite effective elasticity in absence of magnetic field it was assumed that the ferromagnetic spherical particles are evenly and homogeneously distributed in the matrix, hence that the macroscopic response can be obtained from the microscopic model. Assuming each ferromagnetic particles is separated by a distance r_0 from any other ferromagnetic particle in the matrix suspension, the elementary cell representing the material is given by a cube of size r_0 including a ferromagnetic sphere of diameter d. It is also assumed that CIP are evenly distributed in the rubber matrix, no voids are present in the matrix and both of the materials works as linear elastic material. Figure 1 shows the elemental cell considered for the microscopic model, where d is the diameter of the iron particles and r_0 is the distance between them when no magnetic field is applied.

The volume fraction of the iron particles in the rubber matrix, φ, is defined as the ratio of the volume of the ferromagnetic particle over the volume of the elementary cell:

$$\varphi = \frac{\pi d^3}{6r_0^3} = \frac{\pi}{6h^3} \tag{1}$$

where $h = r_0/d$ is an inverse indicator of the gap between two adjacent particles. When there is no ferromagnetic particle φ is zero and $h = \infty$. When spherical particles are

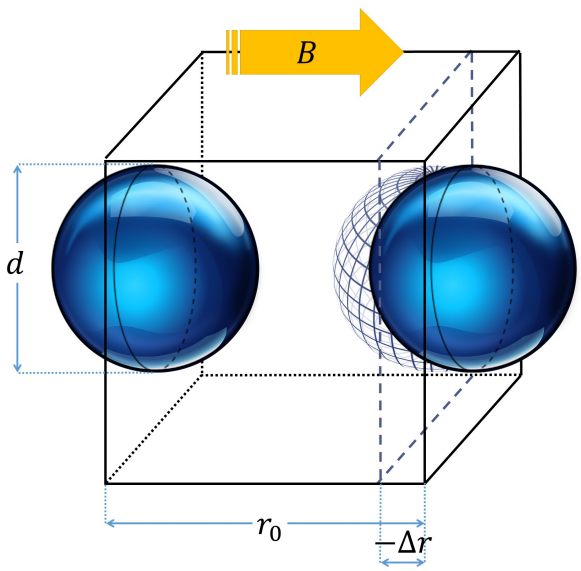

Figure 1. Elementary cubic cell including two iron particle half-spheres evenly distributed in a rubber matrix.

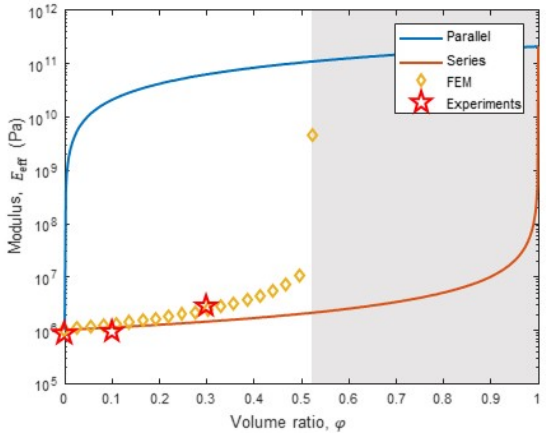

Figure 2. Mixture laws applied to find the effective Young's modulus of the composite. The continuous blue line shows the idealised parallel combination. The continuous red line shows the idealised series connection. The yellow circles and the red stars show the FEM simulation and the experimental results respectively. The grey area is not a feasible area for spherical iron particles.

considered, the maximum admissible φ is $\pi/6 \approx 0.52$ for which $h = 1$.

A mixture law can be used to find the effective macroscopic properties of the MRE material. The effective mass density, ρ_{eff}, is simply related to the CIP volume fraction by

$$\rho_{\text{eff}} = \varphi\rho_{\text{CIP}} + (1-\varphi)\rho_{\text{SR}} \tag{2}$$

where ρ_{CIP} and ρ_{SR} are the densities of the CIP and of the silicone rubber respectively.

In order to find a mixture law for the effective Young's modulus it is important to understand how the load is shared between the matrix and the particles. Given the large number of simplifications already adopted, and wishing to avoid unnecessary and unjustified complication, the parallel and series connections have been considered and taken into account. Figure 2 shows the variation of effective modulus of elasticity as a function of the volume ratio of CIP in MRE φ for the two mixture laws proposed. The material properties of the two materials are given in Table 1. The predictions for series and parallel model are compared in Figure 2 to a mechanical FEM model and to some experimental measures obtained from the samples later described. From the plot it is clear that the series connection provides an approximate estimation of the macroscopic modulus of elasticity with the same order of magnitude as predicted by the FEM and experimental tests. Hence it was decided to use the series formula as prediction of the effective stiffness:

$$E_{\text{eff}} = \frac{E_{\text{CIP}}E_{\text{SR}}}{(1-\varphi)E_{\text{CIP}} + \varphi E_{\text{SR}}} \tag{3}$$

where E_{CIP} and E_{SR} are the Young's modules for CIP and silicone rubber respectively. Furthermore, the validity of the series model is also supported by the fact that higher ranges of particle content are not practical and may not satisfy the following magnetic field interaction model.

Induction curves

The relationship between the magnetic induction B (T=N/Am) and the magnetic intensity H (A/m) is found following the procedure suggested by Jolly et al. (1996) which assumes that the polarisation of the iron particles begin at the polar region and increases towards the centre as the applied field increases. Figure 3 shows a schematic of the unit cell where the matrix is represented in grey and the saturated and unsaturated region in the ferromagnetic particles are indicated by the dark and light blue respectively. In addition to this, the reluctance of the unsaturated region is assumed negligible ($\mu_p \gg 1$), the relative permeability of the matrix and saturated portion of the particle are assumed unity ($\mu_m = \mu_s = 1$) and the flux lines are assumed perpendicular to the secants that define the saturated region. Finally assuming that all the polarisation is due to the iron particles only:

$$B = \mu_0 H + \varphi\langle J_p\rangle \tag{4}$$

where $\langle J_p\rangle$ is the average polarisation density of the iron particles and μ_0 is the vacuum permeability. $\langle J_p\rangle$ is calculated integrating over the saturated and unsaturated regions with the assumption that the magnetic induction in

the saturated portion of the particles is

$$B_s \approx \mu_0 H + J_s \tag{5}$$

where J_s is the saturation magnetisation (for pure iron $J_s = 2.1$ T). Such integration gives an induction relationship:

$$\mu_0 H = \frac{B - \varphi J_s(1-\alpha^3)}{1 + \frac{3}{2}\varphi(\alpha - \alpha^3)} \tag{6}$$

where $\alpha = 2s/d$ is a measure of the non-saturated region. As shown in Figure 3, s measures the unsaturated region and d the diameter of the iron particle. α will be 1 when there is no saturation and at very low applied fields and it will be 0 when all the iron particles are fully saturated.

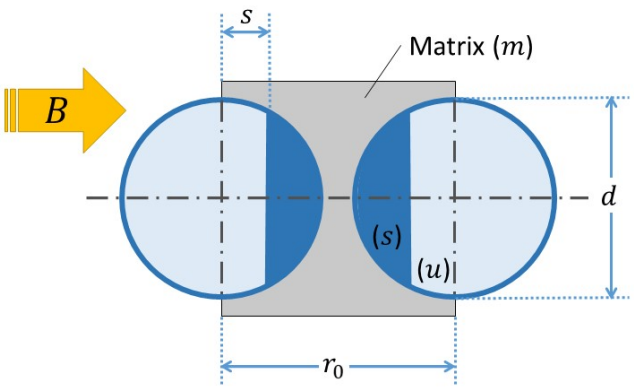

Figure 3. Particle saturation model: (s) region where particle is saturated, (u) region where particle is unsaturated, (m) matrix region.

In order to find α, the magnetic flux circuit through the particles has to be considered. It is assumed the reluctances of the matrix R_m and particles R_p are in parallel and that the magnetic flux (BA) is the same through the saturated and unsaturated region (series connection): $B_p A_p = B_s A_s = B_u A_u$. The magnetic induction flux across the particles $(B_s A_s)$ can be defined as function of the total magnetic flux as

$$B_s A_s = \frac{1}{1 + \frac{R_p}{R_m}} BA \tag{7}$$

where B_s is the magnetic induction in the saturated particles, $A = r_0^2$ is the area of a cell, $A_s = \pi(r^2 - s^2)$ is the area at the saturation threshold. The area ratio can be also expressed as function of the volume ratio and the saturation ratio:

$$\frac{A_s}{A} = \pi(1-\alpha^2)\left(\frac{3}{4}\frac{\varphi}{\pi}\right)^{\frac{2}{3}} \tag{8}$$

while the ratio of reluctances in the matrix and in the particle can be approximated as:

$$\frac{R_p}{R_m} \approx k\frac{2}{\pi(1+\alpha)}\left[\left(\frac{3}{4}\frac{\varphi}{\pi}\right)^{-\frac{1}{3}} - \pi\left(\frac{3}{4}\frac{\varphi}{\pi}\right)^{\frac{1}{3}}\right] \tag{9}$$

where k is a factor added by Jolly et al. (1996) to accommodate for magnetic interaction between adjacent columns and packing arrangements and obtain a better fit to experimental data.

Substituting equations (8), (9), (5) and (6) in equation (7) an implicit function of α is obtained:

$$\begin{aligned}(\mu_0 H + J_s)\left\{\pi(1-\alpha^2)\left(\frac{3}{4}\frac{\varphi}{\pi}\right)^{\frac{2}{3}}\right\} \\ \left\{1 + k\frac{2}{\pi(1+\alpha)}\left[\left(\frac{3}{4}\frac{\varphi}{\pi}\right)^{-\frac{1}{3}} - \pi\left(\frac{3}{4}\frac{\varphi}{\pi}\right)^{\frac{1}{3}}\right]\right\} + \\ - \mu_0 H\left[1 + \frac{3}{2}\varphi(\alpha - \alpha^3)\right] - \varphi J_s(1-\alpha^3) = 0.\end{aligned} \tag{10}$$

The root of equation (10) gives α as function of the magnetic intensity H. Figure 4(a) shows the polarisation ratio α for three values of the volume ratio φ. Hence equation (6) can be used to find the magnetic induction B while equation (4) gives the average polarisation. Figure 4(b) and (c) show the average polarisation $\langle J_p \rangle$ and the magnetic induction B as function of the the magnetic intensity H.

Magnetic stress-strain relationship

Filler particles are considered to be homogeneously distributed in the silicone rubber matrix. When a magnetic field is applied, the ferromagnetic particles are polarised in magnetic dipoles which tend to attract each other. The microscopic individual cell used to study the effect of the magnetic field and the macroscopic constitutive behaviour of the material has been represented by two attracting dipoles as it is shown in Figure 1. The interaction energy E between two dipoles with equal strength, m is given by Jolly et al. (1996); Rosensweig (2013),

$$E = \frac{|m^2|(1 - 3\cos^2\theta)}{4\pi\mu_0\mu_1|r|^3} \tag{11}$$

where $\mu_0 = 4\pi \times 10^{-7}\mathrm{NA}^{-2}$ and μ_1 are the permeability of free space and the relative permeability of the rubber matrix respectively. r is the distance between the two dipoles and θ is the angle between the two dipoles which it is assumed to be zero hereafter. Assuming that the shear deformation is negligible, the distance r between the dipoles can be

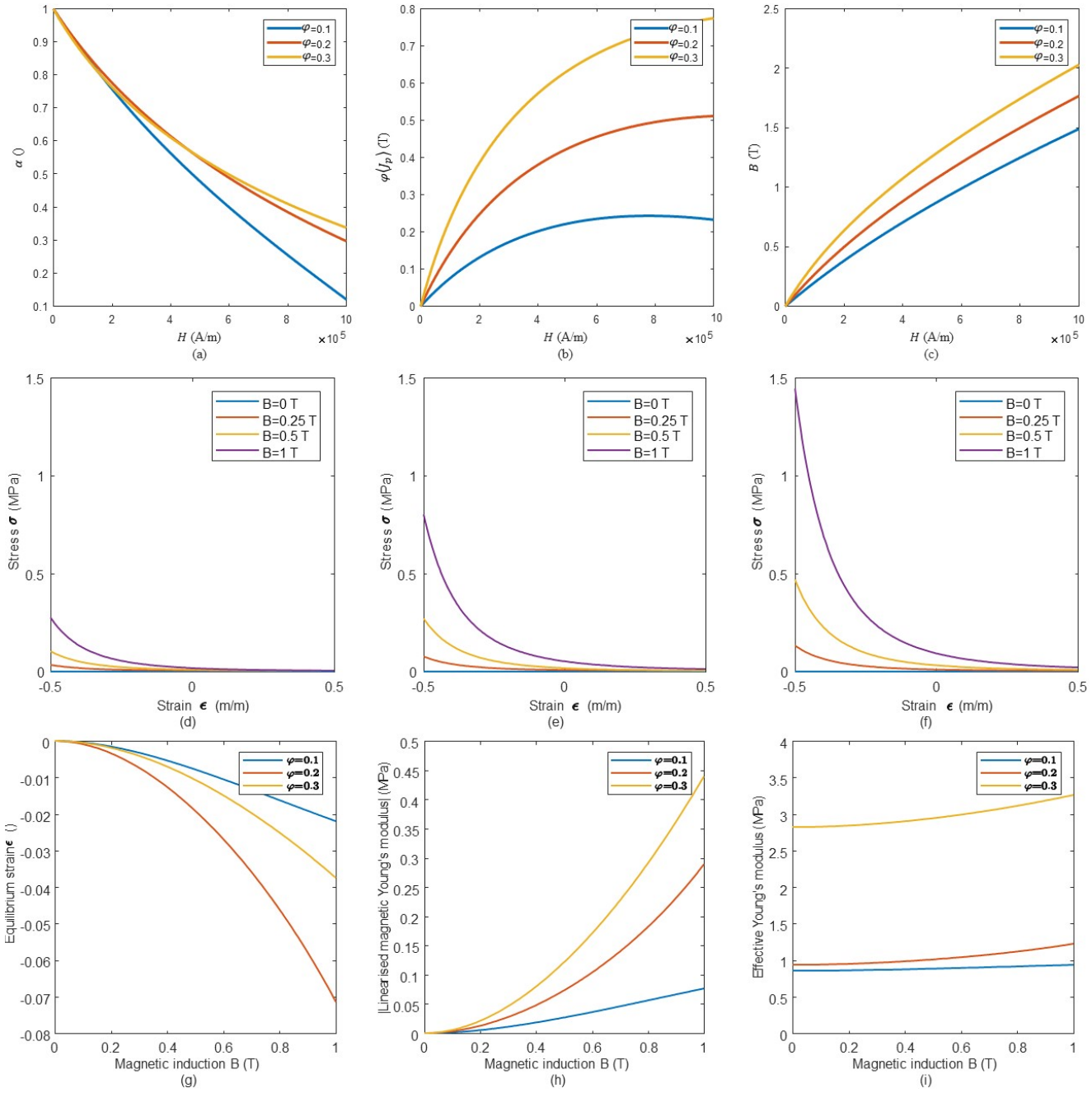

Figure 4. Polarisation curves as function of the the magnetic intensity H for three different values of the volume ratio φ ((a) polarisation ratio α; (b) average polarisation density $\varphi\langle J_p\rangle$; (c) magnetic induction B); Magnetic stress-strain curves at given induced magnetic field B for different volume ratios ((d) $\varphi = 0.1$, (e) $\varphi = 0.2$; (f) $\varphi = 0.3$); Effect of induced magnetic field on (g) static equilibrium strain ε_{eq}, (h) magnetic equivalent linearised Young's modulus $E_{magnetic,lin}$ and (i) effective Young's modulus $E_{\text{tot}} = E_{\text{eff}} + E_{magnetic,lin}$.

expressed as a function of the axial strain $\varepsilon = \Delta r/r_0$

$$r = r_0 + \Delta r = r_0(1+\varepsilon) = dh(1+\varepsilon) \tag{12}$$

Hence E can be simplified and rewritten in terms of scalar strain ε:

$$E = \frac{-|m|^2}{2\pi\mu_0\mu_1 d^3 h^3 (1+\varepsilon)^3} \tag{13}$$

Assuming that the particles are aligned in long chain and there is no multipole interaction, the total energy density U (energy per unit of volume) associated with the one-dimensional strain can be calculated by multiplying the particle-to-particle energy by the total number of particles (N) and dividing by the total volume ($N\frac{\pi d^3}{6}/\varphi$):

$$U = \frac{E\varphi}{(\pi d^3)/6} = \frac{-3|m|^2\varphi}{\pi^2\mu_0\mu_1 d^6 h^3 (1+\varepsilon)^3}. \tag{14}$$

The stress induced by the magnetic field application can be obtained by differentiating U with respect to scalar strain

ε

$$\sigma_{\text{magnetic}} = \frac{\partial U}{\partial \varepsilon} = \frac{9|m|^2\varphi}{\pi^2\mu_0\mu_1 d^6 h^3(1+\varepsilon)^4} \tag{15}$$

Since dipole moments are difficult to measure microscopically, it is more convenient to express dipole moments in terms of the average particle polarisation $\langle J_p \rangle$ as $|m| = \langle J_p \rangle \frac{\pi d^3}{6}$. Hence, the nonlinear magnetic stress-strain relationship can be expressed as:

$$\sigma_{\text{magnetic}} = \frac{3\langle J_p \rangle^2 \varphi^2}{2\pi\mu_0\mu_1(1+\varepsilon)^4} \tag{16}$$

where $\langle J_p \rangle$ can be obtained from equation (4).

Figures 4(d)-(f) shows the stress-strain curves for different values of magnetic induction B and volume ratio φ. The force of interaction reduces, increasing the distance between the magnetic dipoles.

Linearised magnetorheological stiffness

The MRE is composed by CIP in a silicone rubber matrix. An applied magnetic field will cause the CIP magnetic attraction. This is equivalent to an external force acting on the material which will compress the matrix as detailed in the previous section. At the same time, the elastic response of the composite will oppose such magnetic attraction force until the equilibrium state is reached. Considering small displacement around the equilibrium position the combined linearised stiffness can then be calculated. The force equilibrium equation can be written as:

$$\frac{3\langle J_p \rangle^2 \varphi^2}{2\pi\mu_0\mu_1(1+\varepsilon)^4} + E_{\text{eff}}\varepsilon = 0 \tag{17}$$

where it has been assumed a linear constitutive equation for the mechanical stress. E_{eff} can be estimated using equation (3) or it can be measured experimentally from a material sample.

Solving the fifth order polynomial obtained re-arranging equation (17) the equilibrium strain for a given average polarisation can be found :

$$\varepsilon^5 + 4\varepsilon^4 + 6\varepsilon^3 + 4\varepsilon^2 + \varepsilon + \frac{3}{2\pi}\frac{\langle J_p \rangle^2 \varphi^2}{\mu_0\mu_1 E_{\text{eff}}} = 0. \tag{18}$$

Only the one root of the polynomial which falls within the range $-1 \leq \varepsilon \leq 0$ will be considered as the static equilibrium position. Figure 4(g) depicts the variation of equilibrium position against applied magnetic field for different volume ratios φ. Experimental values of E_{eff} obtained from the samples have been used in order to facilitate comparison with the experimental campaign results. Larger magnitude changes of the equilibrium position can be observed as the applied magnetic field is increased.

The relation between $\sigma_{magnetic}$ and ε can be linearly approximated within a small strain range around the equilibrium position ε_{eq} using Taylor's series expansion. Therefore, the factor $(1+\varepsilon)^{-4}$ of $\sigma_{magnetic}$ in equation (16) can be expanded using Taylor's series:

$$(1+\varepsilon)^{-4} \approx (1+\varepsilon_{eq})^{-4} - 4(1+\varepsilon_{eq})^{-5}\Delta\varepsilon \tag{19}$$

where $\Delta\varepsilon = \varepsilon - \varepsilon_{eq}$ is the strain from the equilibrium strain ε_{eq} that accounts for the further MRE deformation after the static equilibrium state is reached. Hence an expression for the linearised magnetic Young's modulus can be obtained

$$E_{magnetic,lin} = \frac{6\langle J_p \rangle^2 \varphi^2}{\pi\mu_0\mu_1(1+\varepsilon_{eq})^5} \tag{20}$$

where the sign has been changed since externally applied forces have to be considered here. Figure 4(h) shows the linearised magnetic Young's modulus as a function of volume concentration and induced magnetic field. Figure 4(i) shows the dependency of the total linearised stiffness of the MRE material, $E_{\text{tot}} = E_{\text{eff}} + E_{magnetic,lin}$, by the induction magnetic field.

Predicted impedance and transmissibility

The MRE samples have been manufactured in a cylindrical form. It is assumed that the MRE cylinders are subject to compressional deformation only and their dynamical behaviour can be mainly represented as that of compressional springs. The total complex stiffness of the sample from the linearised stress equation as $k = (1+\mathrm{i}\eta_{SR})(E_{\text{SR}} + E_{magnetic,lin})\frac{A}{L}$, with η_{SR} is the loss factor of the silicone rubber, A and L the cross-sectional area and height respectively. When employed as adaptive isolators or dynamic vibration absorbers, additional masses representing payload, permanent magnets and electromagnets are added to them. For such applications the MRE sample can be modelled as a stiffness element between two masses m_1 and m_2 as shown in Figure 5. Hence the predicted point impedance for an input force F and velocity $\dot{X}_1$ at the shaker table can be computed as

$$Z = \frac{F_1}{\dot{X}_1} = \frac{(-\omega^2 m_1 + k)(-\omega^2 m_2 + k) - k^2}{\mathrm{i}\omega(-\omega^2 m_2 + k)}, \tag{21}$$

and the transmissibility between base displacement X_1 and mass displacement and X_2 as

$$T = \frac{X_2}{X_1} = \frac{k}{-\omega^2 m_2 + k}. \tag{22}$$

Figure 6 shows the predicted point impedance and transmissibility for the case of 10% and 30% CIP volume ratio and 1 T change in the magnetic induction field. The resonances shift 4.7% for the 10% samples (from 93.7 Hz to 98.17 Hz) and 7.7% for the 30% samples (from 170.6 Hz to 183.7 Hz). Despite the small change in the resonance behaviour of the samples such adaption can still be effectively employed in suitably designed devices. Such results will be compared with the experimental results in the next section giving an insight in the advantages and limitations of the adopted model.

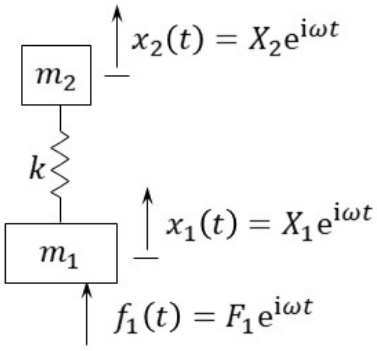

Figure 5. Two DOF system subject to base excitation representing the MRE sample with a payload.

Experimental procedure

This section describes the tests performed to assess the properties of the MRE samples. First, vibration transmissibility and mobility were measured. Then shock isolation properties were measured. An electromagnet (Magnetech opposite pole electromagnet OP-1212) was placed on top of the sample, acting both as an isolated mass of 141 g and as the source of the magnetic field. The electromagnet is cylindrical in shape and both the length and height are 31.75mm. Although the electromagnet shows an internal resonance at about 350 Hz, this is highly damped and it can be effectively considered, in the frequency range of interest, as a rigid mass. It is however important to take the dynamical response of the electromagnet in account for the further design of vibration control devices. The electromagnet was supplied with a DC voltage from a high current source. According to the manufacturer data sheet (Magnetech Corporation 2020) the electromagnet produces an average nominal flux density of 0.075 T when driven at 18 V DC drawing a current of 2.2 A (10% Duty Cycle). In order to increase the magnetic range of investigation one or two permanent magnets (with a mass of 18 g) were placed at the bottom and top of the sample. A limitation of this setup is that due to the size of the MRE sample, the magnetisation may not be uniform. Three different configurations of the sample have been studied and they can be seen in Figure 7. For each configuration driving conditions at different supply voltages were considered. For clarity only a total of five different conditions are going to be reported. Figure 7(a) represents the first configuration of the MRE samples with the electromagnet at the top as payload mass. Condition (a) refers to this configuration with no magnetic field applied. The condition with the electromagnet turned off is considered as the reference basis for other measurements and comparisons. The second configuration, i.e Figure 7(b), sees the MRE sample with one permanent magnet at the bottom of the MRE and the electromagnet at the top. Conditions (b), (c) and (d) refer to this configuration when a supply voltage of 0, 18 and -18 V is provided to the electromagnet respectively. The largest voltage supplied to the electromagnets was $\pm$ 18V to avoid overheating. Figure 7(d) shows a picture of the real sample in this configuration. The final configuration, i.e Figure 7(c), sees the MRE sample with a permanent magnet at the bottom and one at the top. Both magnets were oriented with the same polarity. Condition (e) refers to this configuration when no voltage is supplied to the electromagnet.

Magnetic field measurements

A preliminary measurement of the magnetic field of the permanent magnet and of the electromagnet has been carried out in air. The permanent magnet's magnetic field was measured at 70 mT with a Gaussmeter PCE-MFM 3000. The magnetic field at the electromagnet top was measured with a SS49E linear Hall effect sensor. The measurement was repeated for two available electromagnets. Both electromagnets showed an almost linear relationship between the voltage and the magnetic field with a constant of proportionality of 0.0032 T/V.

Frequency response function results

The MRE sample have been tested as indicated in Figure 7. They were secured to the shaker table via an impedance head and with the electromagnet resting on them. This configuration can be used to measure both their isolation (considering the electromagnet as the payload) and their absorption capabilities (considering the MRE sample and the electromagnet to act as a dynamic vibration absorber). Hence, in order to assess the isolation and absorption properties of the 10% and 30% MRE samples, the impedance and transmissibility were measured for the different conditions described before. The samples were excited by an

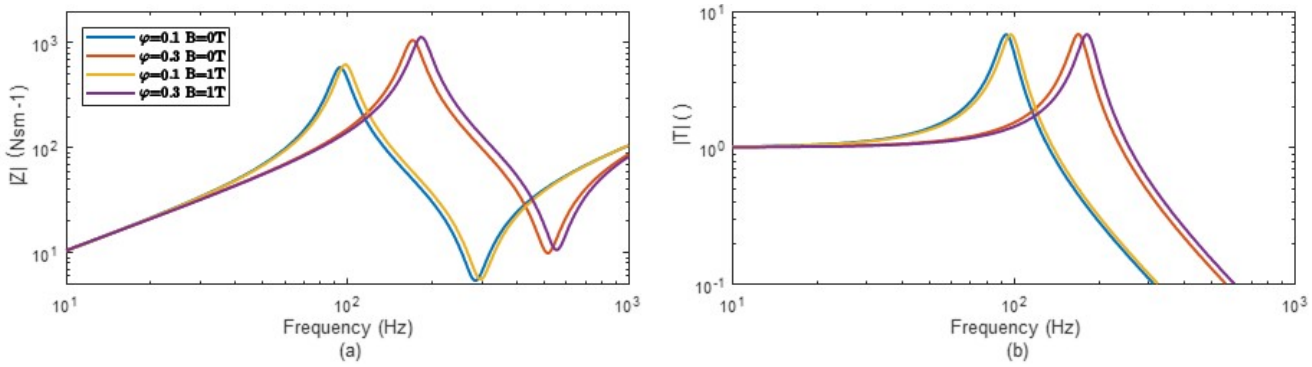

Figure 6. Predicted point impedance (a) and transmissibility (b) for different φ against induced magnetic field.

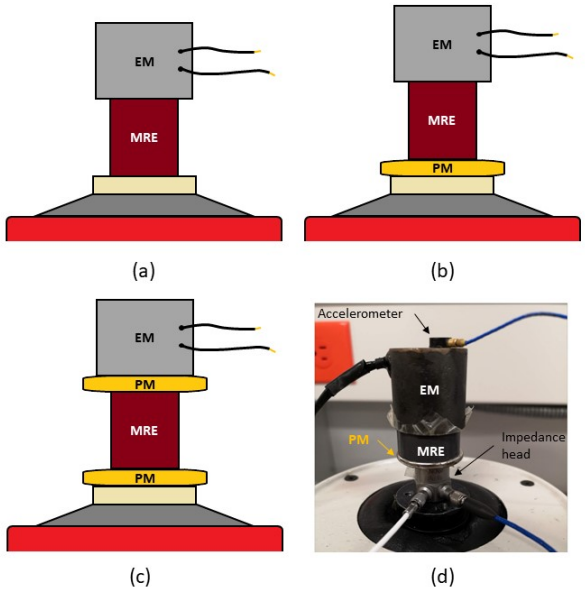

Figure 7. Configurations used in the experimental procedure: (a) MRE sample between the electromagnet and the shaker table; (b) MRE sample with one permanent magnet at its base and electromagnet; (c) MRE sample with two permanent magnets; (d) picture of the actual experimental sample with one permanent magnet

electrodynamic shaker LDS V406, and the input force and acceleration were acquired with an impedance head sensor PCB Piezotronics model 288D01 whilst the transmitted acceleration on top of the electromagnet was measured with a miniature accelerometer PCB Piezotronics 352C22. The samples were excited by a broadband random excitation up to 500 Hz through the shaker. The amplitude of the input signal was kept constant during the tests at about 1.5 g (rms) to assure linearity which was confirmed by the measured coherence function. The signals from the impedance sensor and the accelerometer were acquired through dynamic signal analyser Dataphysics QUATTRO. It is important to mention that the tests were performed at constant room temperature to avoid changes in stiffness and damping due to viscoelastic effects. It is also known that stiffness and damping in rubbers change with frequency, but since only a relatively short frequency range is analyzed in the test under random excitation and not cyclic loading, this effect was not taken into account. The tests were repeated twice swapping the face of the permanent magnet. In order to observe the largest frequency changes, some examples of the impedance and transmissibility functions are presented in Figure 8. For those voltages, the largest frequency changes are obtained whilst when the electromagnet is turned off the natural frequency falls in the middle. When the bottom permanent magnet is completely removed the resulting natural frequency is the lowest registered, effectively measuring the properties of the sample with no magnetic effect.

In addition, the properties of the silicon rubber sample with no CIP, i.e. 0% were measured, resulting in a natural frequency of 90.83 Hz, and viscous damping ratio of 0.0743. On the other hand, Table 2 presents the calculated values of natural frequencies and loss factor for the 10 % and 30% samples respectively. The data was processed using a circle fit of the impedance measurements, for the different conditions considered, i.e. case (a) for the samples with no permanent magnet (PM) and the electromagnet (EM) turned off, cases (b) with the permanent magnet at the bottom and voltages of +18 V and -18 V supplied to the electromagnet, and lastly two permanent magnets with the electromagnet turned off acting only as payload. These scenarios are summarised on Table 2 together with the percentage change in the stiffness and measured natural frequency. The stiffness change was estimated considering case (a) as reference for comparison, i.e. the electromagnet turned off without the permanent magnet at the bottom.

Assuming the magnetic field is due to the superposition of the magnetic fields, generated in vacuum from the permanent magnet and the electromagnet, it is possible to estimate the variation of the Young's modulus of the MRE samples. In other words it has been assumed that the ferromagnetic particles in the sample do not alter the magnetic field and that

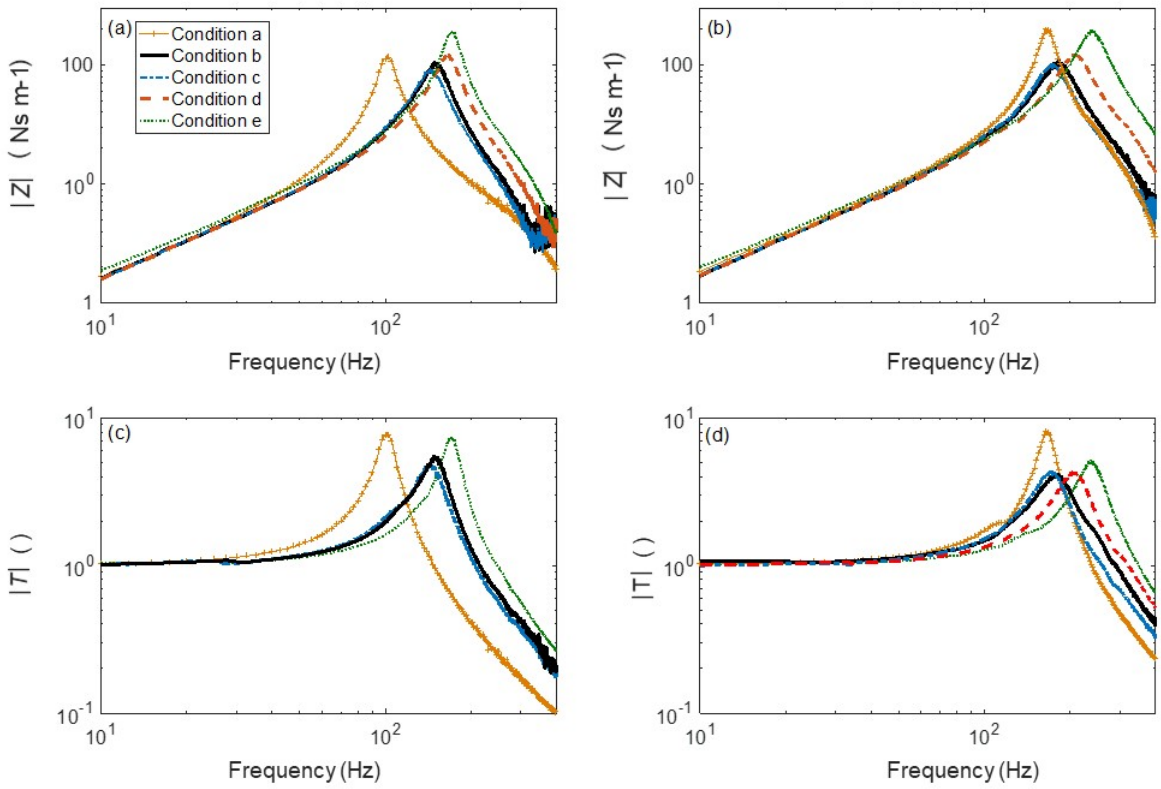

Figure 8. Frequency response functions of the MRE isolator (a) Mechanical impedance 10% sample, (b) mechanical impedance 30% sample, (c) absolute transmissibility 10% sample, (c) absolute transmissibility 30% sample

Table 2. Values of natural frequency in Hz, damping ratio, and stiffness change measured for different configurations of the MRE sample with 10% and 30% of particles concentration. (PM: permanent magnet; V_{EM}: voltage supplied to the electromagnet.)

	B (T)	f_n (Hz)		ζ		% Δk	
a. No PM, $V_{EM} = 0$ V	0	98	168	0.1148	0.1309		
b. 1 PM, $V_{EM} = 0$ V	0.07	150	180	0.1105	0.1551	57.315	12.888
c. 1 PM, $V_{EM} = 18$ V	0.127	164	214	0.0945	0.0961	64.292	38.370
d. 1 PM, $V_{EM} = -18$ V	0.013	143	174	0.1065	0.0858	53.034	6.777
e. 2 PMs, $V_{EM} = 0$ V	0.14	175	247	0.1016	0.0801	68.640	53.737
Particle concentration φ (%)		10	30	10	30	10	30

the stiffness of the sample is related to the Young's modulus as $k = EA/L$ where A and L are the cross-sectional area and height of the sample. The results of the Young's modulus estimation is presented in Figure 9. Comparing Figure 9 with Figure 4(i), it is clear that the model suggested here describes the change of the effective Young's modulus due to the magnetic field only up to about 0.08 T. For larger magnetic field the magnetic compression seems to produce a stiffening in the samples, which is probably due to the hyper-elastic response of the composite. This also explains why the model predicts that the resonance shift would happen over a larger change in the magnetic induction field.

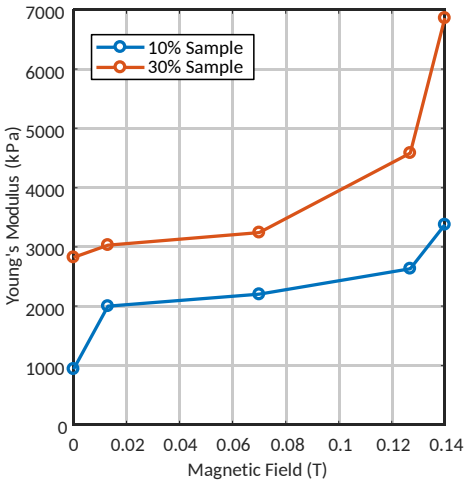

Figure 9. Experimentally estimated variation of the Young's modulus with the magnetic field.

The variation of isolation properties was also evaluated for different values of the supplied voltage. For this experiment, the voltage was varied from -18 V to +18 V in 9 V steps, for

two conditions of the permanent magnet at the bottom, i.e. for condition 1 the positive pole (or face 1) of the magnet was facing up, while in condition 2 the face was swapped, i.e. negative pole facing up. The change of natural frequency as a function of the supplied voltage is presented in Figure 10, for the two samples considered and the two conditions of the permanent magnet. Thus, it can be seen that when the polarity of the permanent magnet is inverted by swapping the face, the trend in the variation of the natural frequency is also reversed as a result.

Shock response results

Shock response was evaluated experimentally by applying a velocity compensated half sine acceleration pulse in the base of the system. The pulse was generated by the data acquisition software and applied through the electrodynamic shaker. The rest of the experimental setup was the same as the previous stage. Pulse durations of 1 ms, 5 ms, 10 ms, 15 ms and 20 ms were considered to cover the different areas typically found in the shock response of a linear system, i.e. pulses shorter than the natural period, around the natural period, and larger than the natural period. The amplitude of the pulse $\ddot{y}_p = \ddot{x}_1$ in all cases was kept constant to 1 g acceleration. For the shock response, only the 30% particle volume concentration sample was studied since it gives the largest stiffness changes for the different configurations. Figure 11 presents the time response for the different configurations of the MRE studied, where each subplot gives a particular pulse duration. The response amplitude $\ddot{x}_2$ is normalised by the shock amplitude $\ddot{y}_p$.

The maximum value of the absolute response is compared to the maximum input amplitude, and presented as a function of the period ratio between the duration of the pulse τ and the natural period of the system T in Figure 12. For this plot, the natural period of the MRE sample with no permanent magnet and the electromagnet turned off (case a), i.e. approximately 5 ms for the 30% sample was considered as a reference.This effectively represents the shock response spectra, and it is presented for the different configurations of the MRE.

Discussion of experimental findings

The mobility function and transmission ratio presented in Figure 8 show the effect of change in the natural frequency of the isolator sample. First, the effect of the particle percentage is clearly seen. Compared to the sample with 0% CIP concentration which has a natural frequency of 90.83 Hz, the stiffness change due to the addition of the particles is 14% and 71% for the 10% and 30% samples respectively. When comparing the 10% and 30% samples without any magnetic effect (case a) the natural frequencies are 98 Hz and 168 Hz respectively resulting in a change of stiffness of approximately 66%. This obeys to the fact of increased stiffness due to the higher concentration of particles as expected. However, the main objective is to compare the effect of different magnetic fields applied to the sample. The initial value for comparison as a reference is considered when the bottom permanent magnet is in place and the electromagnet is turned off effectively acting as a payload, i.e. condition (b). The effective natural frequency for this state is 150 Hz and 180 Hz for the the 10% sample and the 30% sample respectively. The frequency is increased to 164 Hz and 214 Hz in each sample when a positive voltage is applied, resulting in a stiffness increase of 64% and 38%. On the other hand, a negative voltage produces a decrease in the frequency, corresponding to 143 Hz and 174 Hz respectively. The actual stiffness changes from minimum to maximum stiffness for each sample results in 53% and 7% for the 10% and 30% samples respectively, when considering condition (a) as a baseline. However, for practical implications, if condition (b) is taken as a reference, then by switching on and off the electromagnets in reverse polarities the stiffness can be increased and reduced from the baseline, which can be useful for further control strategies where it is important to have the largest stiffness change possible from a minimum to a maximum value.

A practical limit of the electromagnets used on the experiments was the maximum voltage, current and time of operation. Due to the high current drawn at 18 V, they experienced a quick overheating. Thus it was not possible to sustain the tests for higher voltages and longer times. Additionally, this will also affect the total mass of the system since increasing the magnetic field, i.e. by using a stronger electromagnet, will result in a larger and heavier system, thus limiting practical applications. However, the feasibility of quickly changing the effective stiffness of the system was shown in the tests. In order to observe larger stiffness changes, permanent magnets were used. In this case, the maximum natural frequencies recorded were 175 Hz and 247 Hz for the 10% and 30% respectively, and considering the initial sample with no magnetic effects as reference, the actual stiffness increase was 68% and 53% for each sample.

A comparison with the predicted stiffness values is presented in Table 3 for the 10% and 30% samples. Theoretical stiffness is calculated from the Young modulus values presented in Figure 9 as $k = EA/L$, whilst experimental stiffness is estimated from the natural frequencies discussed in Table 2 and the payload mass.

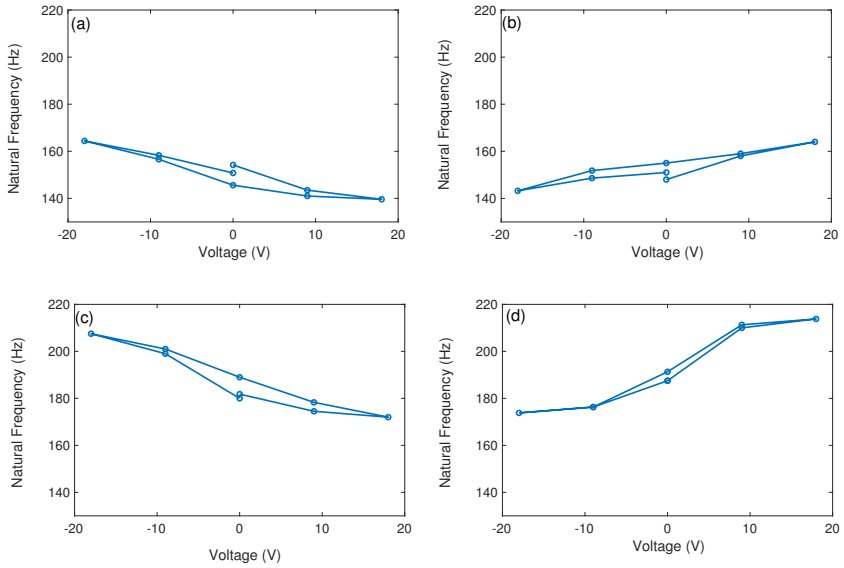

Figure 10. Effect of the applied voltage in the natural frequency of the MRE sample. (a) 10% sample face 1, (b) 10% sample face 2, (c) 30% sample face 1, (d) 30% sample face 2

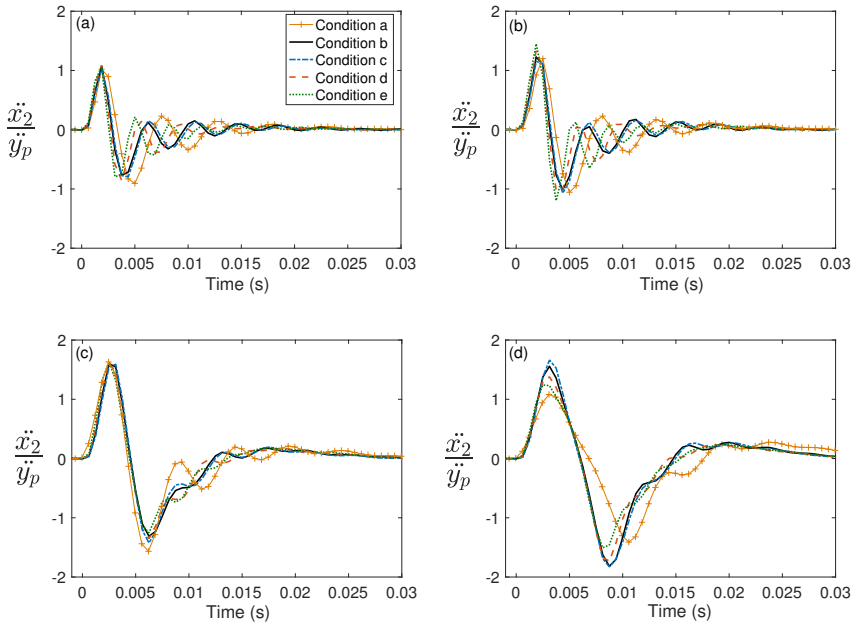

Figure 11. Shock response of the MRE isolator considering the 30% sample (a) 1 ms, (b) 5 ms, (c) 10 ms, (d) 15 ms.

Only three values fo applied magnetic field are included for brevity, i.e. 0 T, 0.07 T and 0.14 T. It can be seen that the predictions provide acceptable results useful for later implementations. However, the difference becomes large with higher magnetic fields, probably due to the limitations in the experimental testing, i.e. magnetisation not uniform, and previously discussed simplifications in the model.

Table 3. Comparison of the theoretically predicted stiffness and the experimental results.

B (T)	k_{theory} (N/m)		k_{exp} (N/m)		error %	
0	58905	170824.5	53081	155993	10.4	9
0.07	129591	188496	124357	179074	4.1	5.1
0.14	200277	412335	169263	337195	16.8	20
φ (%)	10	30	10	30	10	30

The shock isolation results also agree with previous findings and are not surprising as a system with lower stiffness results in a better shock isolation for short pulses compared to the duration of the pulse, i.e. $\frac{\tau}{T} < 2$. Only the

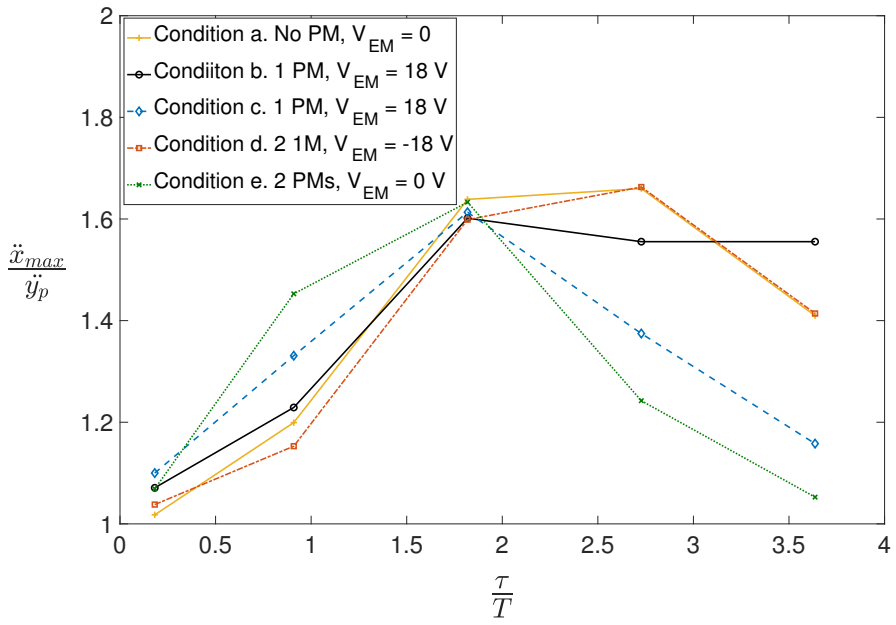

Figure 12. Shock response spectra of the MRE isolator considering the 30% sample for the different configurations considered.

30% sample was studied in this experiments, since it is the one with the largest stiffness change considering case (b) as a reference, and as a consequence larger differences in shock response can be appreciated. In this case, the higher effects in the response were observed for the 5 ms, 15 ms and 20 ms pulses. For example, in the case of the 5 ms pulse, considered short compared to the natural period, the shock response decreases approximately 6% for the lower stiffness value corresponding to a supply voltage of -18 V, and increases 8% for the larger stiffness at 18 V, taking case (b) as baseline. For longer pulses, $\frac{\tau}{T} > 2$ the opposite effect is observed as a lower stiffness increases the response and a higher stiffness decrease the response. This effect is due to the system approaching the amplification region, i.e. by reducing the stiffness, the relative shock duration to system natural period ratio decreases and it is moved towards the amplification region in the shock response spectra. Increasing the stiffness moves the effective period ratio towards the quasi-static zone resulting in a longer pulse compared to the duration of the shock. When using both permanent magnets the effects discussed are observed at a larger magnitude. However, this proves useful for further use in a switchable stiffness strategy as previous studies have suggested, or even the implementation of a two stage mount with switchable stiffness.

Conclusions

The design and modeling of simple vibrations isolators using magnetorhelogical elastomers was presented and discussed. Even though the use of MRE is relatively well understood for vibration isolation and suppression this paper attempts to present a simple yet functional model for axial configurations. Based on the properties of the individual components, i.e. the silicon rubber matrix, and the carbonyl iron powder the Young Modulus of the mixture was established. Then, the magnetic effects were investigated, finding polarisation curves as a function of the volume ratio between the particles and the matrix, and stress strain relationships under the effect of the magnetic field for the same particle concentrations. Finally, a linearised stiffness was predicted for the MRE samples based on the Young modulus of the mixture, and the magnetic Young modulus. The model is limited to the linear elastic response and does not model the hardening which happens for large magnetic induction fields. A compensation for this limit has been obtained increasing the simulated induction field. Vibration transmissibility and mobility were calculated for different particle concentrations and magnetic field values. Then, MRE samples were manufactured in different particle concentrations and the change of stiffness was assessed under different magnetic field levels in shaker testing. Vibration transmissibility and mechanical impedance were experimentally measured, finding that it is possible to obtain a significant stiffness change of up to 64% which is controllable by by changing the magnitude and polarity of the voltage supplied to the electromagnets. Shock response was also evaluated, finding better isolation for low stiffness states. The proposed procedure is simple but it allows to estimate the stiffness of a MRE sample for different

percentages of CIP volume concentration as a function of the applied magnetic field. Estimating theoretically the minimum and maximum stiffness of MRE samples can prove useful in designing switchable stiffness strategies. In addition, the properties of the experimentally developed samples, i.e. a large change in stiffness in a very short time, makes them suitable for use in further stiffness switching strategies for vibration isolation and suppression.

Funding Acknowledgement

The authors would like to acknowledge the 'Mexico-UK Visiting Chair' mobility funding between the University of Southampton and the Universidad Autonoma de Nuevo León for the support provided in the development of this project.

Conflict of Interest

The authors declare no conflict of interest in preparing this article.

References

Blom, P. and Kari, L. (2005) "Amplitude and frequency dependence of magneto-sensitive rubber in a wide frequency range" in: Polymer testing, 24(5), 656–662

Blom, P. and Kari, L. (2012) "The frequency, amplitude and magnetic field dependent torsional stiffness of a magnetosensitive rubber bushing" in: International Journal of Mechanical Sciences, 60(1), 54–58

Borcea, L. and Bruno, O. (2001) "On the magneto-elastic properties of elastomer–ferromagnet composites" in: Journal of the Mechanics and Physics of Solids, 49(12), 2877–2919

Brigadnov, I. and Dorfmann, A. (2003) "Mathematical modeling of magneto-sensitive elastomers" in: International Journal of Solids and Structures, 40(18), 4659–4674

Bustamante, R. (2010) "Transversely isotropic nonlinear magnetoactive elastomers" in: Acta mechanica 210(3-4), 183–214

Carlson, J. D. and Jolly, M. R. (2000) "Mr fluid, foam and elastomer devices" in: Mechatronics 10(4), 555–5694

Castañeda, P. P. and Galipeau, E. (2011) "Homogenization-based constitutive models for magnetorheological elastomers at finite strain" in: Journal of the Mechanics and Physics of Solids 59(2), 194–215

Chen, L. and Jerrams, S. (2011) "A rheological model of the dynamic behavior of magnetorheological elastomers" in: Journal of Applied Physics 110(1), 013513

Danas, K., Kankanala, S. and Triantafyllidis, N. (2012) "Experiments and modeling of iron-particle-filled magnetorheological elastomers" in: Journal of the Mechanics and Physics of Solids 60(1), 120–138

Davis, L. (1999) "Model of magnetorheological elastomers" in: Journal of Applied Physics 85(6), 3348–3351

Deng, H.-X. and Gong, X.-L. (2008) "Application of magnetorheological elastomer to vibration absorber" in: Communications in nonlinear science and numerical simulation 13(9), 1938–1947

Dorfmann, A. and Ogden, R. (2004) "Nonlinear magnetoelastic deformations of elastomers" in: Acta Mechanica 167(1-2), 13–28

Dyniewicz, B., Bajkowski, J. M. and Bajer, C. I. (2015) "Semiactive control of a sandwich beam partially filled with magnetorheological elastomer" in: Mechanical Systems and Signal Processing 60-61, 695 – 705

Eshaghi, M., Sedaghati, R. and Rakheja, S. (2016) "Dynamic characteristics and control of magnetorheological/electrorheological sandwich structures: A state-of-the-art review" in: Journal of Intelligent Material Systems and Structures 27(15), 2003–2037

Han, Y., Hong,W. and Faidley, L. E. (2013) "Field-stiffening effect of magneto-rheological elastomers" in: International Journal of Solids and Structures 50(14), 2281–2288

Jolly, M. R., Carlson, J. D. and Munoz, B. C. (1996) "A model of the behaviour of magnetorheological materials" in: Smart Materials and Structures 5(5), 607

Landi, L., Szmidt, T., Pisarski, D., Konowrocki, R., Awietjan, S. and Boczkowska, A. (2019) "Adaptive damping of a double-beam structure based on magnetorheological elastomer" in: Shock and Vibration 2019, 8526179

Ledezma-Ramirez, D., Ferguson, N. and Brennan, M. (2011) "Shock isolation using an isolator with switchable stiffness" in: Journal of Sound and Vibration 330(5), 868 – 882

Ledezma-Ramirez, D., Ferguson, N. and Brennan, M. (2012) "An experimental switchable stiffness device for shock isolation" in: Journal of Sound and Vibration 331(23), 4987 – 5001

Li, R. and Sun, L. (2014) "Dynamic viscoelastic modeling of magnetorheological elastomers" in: Acta Mechanica 225(4-5), 1347–1359

Li, Y., Li, J., Li,W. and Du, H. "A state-of-the-art review on magnetorheological elastomer devices" in: Smart materials and structures 23(12), 123001

Lokander, M. and Stenberg, B. (2003) "Performance of isotropic magnetorheological rubber materials" in: Polymer Testing 22(3), 245–251

Magnetech Corporation (2020) "DC opposite pole electromagnets" in: http://www.magnetechcorp.com/opposite_pole.html, accessed: 29-05-2020

Rosensweig, R. E. (2013) “Ferrohydrodynamics” by Courier Corporation

Schubert, G. (2014) “Manufacture, characterisation and modelling of magneto-rheological elastomers”, PhD thesis, University of Glasgow

Shen, Y., Golnaraghi, M. F. and Heppler, G. (2004) “Experimental research and modeling of magnetorheological elastomers” in: Journal of Intelligent Material Systems and Structures 15(1), 27–35.

Stepanov, G., Abramchuk, S., Grishin, D., Nikitin, L., Kramarenko, E. Y. and Khokhlov, A. (2007) “Effect of a homogeneous magnetic field on the viscoelastic behavior of magnetic elastomers” in: Polymer 48(2), 488–495

Wang, D., Chen, J.-S. and Sun, L. (2003) “Homogenization of magnetostrictive particle-filled elastomers using an interface-enriched reproducing kernel particle method” in: Finite elements in Analysis and Design 39(8), 765–782

Wang, Y., Hu, Y., Chen, L., Gong, X., Jiang, W., Zhang, P. and Chen, Z. (2006) “Effects of rubber/magnetic particle interactions on the performance of magnetorheological elastomers” in: Polymer Testing 25(2), 262–267

Yin, H. and Sun, L. (2005) “Magnetoelasticity of chain-structured ferromagnetic composites” in: Applied Physics Letters 86(26), 261901

Yin, H., Sun, L. and Chen, J. (2002) “Micromechanics-based hyperelastic constitutive modeling of magnetostrictive particle-filled elastomers” in: Mechanics of materials 34(8), 505–516

Yin, H., Sun, L. and Chen, J. (2006) “Magneto-elastic modeling of composites containing chain-structured magnetostrictive particles” in: Journal of the Mechanics and Physics of Solids 54(5), 975–1003